Nanoscale

CVD Growth of Large-Area InS Atomic Layers and Device Applications

Journal:	*Nanoscale*
Manuscript ID	NR-COM-02-2020-001104.R2
Article Type:	Communication
Date Submitted by the Author:	02-Apr-2020
Complete List of Authors:	Tu, Chien-Liang; National Sun Yat-sen University, Department of Electrical Engineering Lin, Kuang-I; National Cheng Kung University, Center for Micro/Nano Science and Technology Pu, Jiang; Nagoya University, Department of Applied Physics Chung, Tsai-Fu; National Taiwan University, Department of Materials Science and Engineering Hsiao, Chien-Nan; National Applied Research Laboratories, Taiwan Instrument Research Institute Huang, An-Ci; National Sun Yat-sen University, Department of Electrical Engineering Yang, Jer-Ren; National Taiwan University, Department of Materials Science and Engineering Takenobu, Taishi; Nagoya University, Department of Applied Physics Chen, Chang-Hsiao; National Sun Yat-sen University, Department of Electrical Engineering

CVD Growth of Large-Area InS Atomic Layers and Device Applications

*Chien-Liang Tu, Kuang-I Lin, Jiang Pu, Tsai-Fu Chung, Chien-Nan Hsiao, An-Ci Huang, Jer-Ren Yang, Taishi Takenobu, and Chang-Hsiao Chen**

C.-L. Tu, A.-C. Huang, Prof. C.-H. Chen
Department of Electrical Engineering, National Sun Yat-sen University, Kaohsiung 80424, Taiwan
E-mail: chchen@mail.ee.nsysu.edu.tw
Dr. K.-I Lin
Center for Micro/Nano Science and Technology, National Cheng Kung University, Tainan 70101, Taiwan
Prof. J. Pu, Prof. T. Takenobu
Department of Applied Physics, Nagoya University, Nagoya 464-8603, Japan
Dr. T.-F. Chung, Prof. J.-R. Yang
Department of Materials Science and Engineering, National Taiwan University, Taipei 10617, Taiwan
Dr. C.-N. Hsiao
Taiwan Instrument Research Institute, National Applied Research Laboratories, Hsinchu 30076, Taiwan

Keywords: Indium sulfide, InS, CVD, 2D materials, Field-effect transistor

Abstract

Group-III monochalcogenides of two-dimensional (2D) layered materials have attracted widespread attention among scientists due to their unique electronic performance and interesting chemical and physical properties. Indium sulfide (InS) is attracting increasing interest from scientists because it has two distinct crystal structures. However, studies on the synthesis of highly crystalline, large-area, and atomically thin-film InS have not been reported thus far. Here, the chemical vapor deposition (CVD) synthesis method of atomic InS crystals has been reported. The direct chemical vapour phase reaction of metal oxides with chalcogen precursors to produce a large-sized hexagonal crystal structure and atomic-thickness InS flakes or films. The InS atomic films are merged with a plurality of triangular InS crystals that are uniform and entire, have surface areas of 1 cm^2 and controllable thicknesses in bilayers or trilayers. The properties of the as-grown highly crystalline samples were characterized by spectroscopic and microscopic measurements. The ion-gel gated InS field-effect transistors (FETs) reveal n-type transport behavior, and have an on-off current ratio of > 10^3 and a room-temperature electron mobility of ~ 2 cm^2/Vs. Moreover, our CVD InS can be transferred from mica to any substrates, so various 2D materials can be reassembled into vertically stacked heterostructures, thus facilitating the development of heterojunctions and explorations of the properties and applications of their interactions.

1. Introduction

The MX group-III monochalcogenides, wherein M is a group-IIIA metal atom (Ga or In) and X is a group-VIA chalcogenide atom (S or Se), have received increasing interest beyond transition-metal dichalcogenide (TMDC), particularly as it is promising for next-generation electronic and optoelectronic alternatives.[1-4] Monolayer 2D layered group-III monochalcogenides have a hexagonal lattice constructed in an X-M-M-X arrangement in which both group-IIIA metal-atom planes are sandwiched between both chalcogenide-atom planes through covalent bonds; each quadruple layer is stacked with van der Waals bonds.[5]

Indium sulfide (InS) is an n-type compound semiconductor that belongs to this family. The bulk InS has an indirect band gap of 1.9 eV and the monolayer form can increase to ~2.7 eV,[6-8] which modulates the bandgap depending on the layer number, making it a promising candidate for next-generation transistors and optoelectronics. Moreover, InS has a light electronic effective mass of 0.26 m_0,[7] resulting in a Hall mobility of ~50 cm^2/Vs at room temperature.[8] However, unlike the most famous member of the group-III monochalcogenides, indium selenide (InSe),[9-11] InS-related reports are rather rare due to the difficulty of synthesizing InS single crystals.[12, 13] It is worth noting that InS has been found to have two different crystalline phases, which belong to the network and layered structural forms, respectively.[14] Although each is composed of fundamental S-In-In-S units, network InS has lower-energy, a stable state, and its unit is

arranged in an orthorhombic crystal structure. On the other hand, layered InS exhibits higher energy, a metastable state, and a hexagonal structure.

Recently, some studies have shown that, regardless of form, InS can be synthesized into bulk crystals by using methods such as physical vapor transport (PVT) or catalyzed synthesis,[12-15] and these InS crystals exhibit many unusual characteristics. Furthermore, Zavrazhnov et al. have reported a typical In–S binary phase diagram,[16, 17] which showed that InS has complex stoichiometric ratios, such as InS, In_6S_7, In_3S_4, and In_2S_3. The diagram shows that the synthesis of different compounds in the In–S system depends on the temperature, and that suitable growth temperature for InS crystals is between 642 and 691 ℃. However, most of these InS forms are based on bulk morphology with uncontrollable thickness and random lateral dimensions, making them unsuitable for use as transparent, flexible, and ultra-short channels for next-generation nanoelectronics. Nevertheless, next-generation electronic devices require artificial films of atomically thin, highly crystalline, and large-sized 2D semiconductors.[18, 19]

To the best of my knowledge, the CVD growth of highly crystalline, large-sized InS atomic layers has not yet been researched. According to our previous CVD InSe works,[20] in this study we developed a CVD method to synthesize atomic-layer and highly crystalline InS flakes on a mica substrate by injecting two masses of precursor-assisted vapors in a hot-wall horizontal reactor. X-ray photoelectron spectroscopy (XPS) and confocal Raman spectroscopy confirmed

the stoichiometry and characteristic peaks of the CVD InS samples. Comparisons of high-angle annular dark-field scanning transmission electron microscopy (HAADF STEM), atomic force microscopy (AFM), and scanning electron microscopy (SEM) scans show that our InS flakes have a 2D layered structure and a high degree of crystallinity. Of particular note is that the electrical measurements indicate that FETs based on CVD InS atomic layers have unipolar n-type behaviors and moderate mobility performance.

2. Results and Discussion

We performed the direct growth of 2D InS atomic layers on a mica by reacting indium (III) oxide (In_2O_3) and sulfur (S) vapors in a precursor-assisted CVD (see Supporting Information, Methods). Figure 1a depicts the CVD InS experimental setup schematically. In the InS synthesis process, hydrogen (H_2) and argon (Ar) act as reductant and carrier gas, respectively. Freshly cleaved fluorphlogopite mica was employed to grow 2D InS flakes due to its outstanding van der Waals epitaxy substrate with a smooth and inert surface. Figure 1b illustrates an InS layer composed of an S–In–In–S crystal structure. Figure 1c reveals the AFM-scanned image for the bilayer InS triangular crystals, which are approximately several tens of microns in the lateral size. Its bilayer thickness of ~1.7 nm is consistent with the theoretical calculation of monolayer InS thickness of ~0.82 nm.[21, 22] The triangular form of the synthesized InS bilayers was changed according to the growth time. Figures 1d–f reveal low-magnification SEM images of the as-grown InS at growth times of 3, 5, and 10 min, respectively, to show the

various morphologies of the wide-ranging InS population. Over time, the small triangular InS flakes were rearranged and aggregated into large single-crystal InS flakes. It is worth noting that the InS nucleation density depends on the growth position, and two types of shapes were exhibited for the synthesized InS according to the amount of space between the mica and indium vapor. Figure 1g reveals a high-magnification optical microscope (OM) image for transferred bilayer InS flakes. The triangular morphology is usually located at the furthest substrate from the indium vapor (5–7 cm), which means that this interval has low-density nucleation. Further, the average horizontal size of triangular InS can be up to ~50 μm. Figure 1h displays the InS grown near the indium vapor (1–3 cm) where it naturally merges into large-area, continuous, and uniform thin films. Figure 1i is a photo of large-area InS merged films on 1 cm^2 transparent mica. We can see the text below the InS films showing its excellent light transmission. Furthermore, the direction of small-sized InS crystals aligns with specific orientations such as 0° and 60° in the early stage of synthesis, which means that the epitaxial growth mechanism was dominant, as shown in Figure S1. In epitaxial growth, the stability of flakes or nano-clusters on a substrate is critical. Overall, the interaction between InS flakes and SiO_2 (or sapphire) is not as stable as that between InS flakes and mica. As shown in Figure S2, the sapphire substrate generates a large number of particles, while the SiO_2 substrate is prone to forming disordered samples. Remarkably, it shows that the mica substrate with moderate interaction and lattice-matching epitaxy can stabilize 2D InS flakes in a growth time scale. Moreover, it is worth

noting that the temperature can be controlled between 650–690℃ and that this range can stably grow the atomic layer InS. However, once the synthesis temperature exceeds 725 ℃, the appearance of the synthesized samples will quickly stack up and become very messy, as shown in Figure S3. XPS analysis showed that In:S atomic ratio of this In–S compound was close to 46:54, which was confirmed to be In_6S_7. Therefore, according to the In–S phase diagram[16, 17] and the actual synthesis results, the growth temperature is a very important key point for InS synthesis.

Figure 2a shows that the trilayer InS are stacking layers added to some of the bilayer flake tops. Figure 2b displays that the extra layer on top of the bilayer InS is a monolayer through AFM analysis, while obtaining the height and cross-section profile of two kinds of InS flakes. In addition, these trilayer InS flakes appear occasionally, which indicates that these areas have a rough surface. In addition, monolayer (1L) InS flakes were synthesized on the mica substrate, as shown in Figure S4. The AFM image shows that the monolayer InS has a horizontal length of about <2 μm and will only appear on samples with an independent island-like appearance. However, monolayer InS samples are very unstable during synthesis. When the samples are driven by high temperature, once islands contact each other, they merge and quickly grow into a second layer and stabilize. Therefore, under the various trade-offs of InS size, sample analysis, and electrical device preparation, the bi- and trilayer InS architectures were focused on in this

paper. Figure 2c shows that the as-grown bi- and trilayer InS flakes exhibit three characteristic peaks including A^1_g at 151 cm^{-1}, A^4_g at 225 cm^{-1}, and A^2_g at 318 cm^{-1}, which confirms that they are InS materials.[13, 15, 23, 24] Generally, relative vibration and interlayer interaction depends on the layered material. The bilayer and trilayer InS show related Raman peaks; therefore, as-grown CVD InS really has a layered structure. In addition, the lower peak intensity is due to its thin thickness.[25] As reported elsewhere,[26, 27] we avoid further interference from the Raman peaks of mica by using a PMMA-mediated wet process to transfer the CVD InS flakes from mica to SiO_2 substrates (see Supporting Information, Methods). Furthermore, using optical absorption spectra is useful to obtain the band gap energy of 2D materials.[28] The optical absorption experiments require InS samples to have a large area and maintain a uniform thickness. Depending on the size of the laser spot, the area of the uniform film is at least 1 x 2 mm. In order to assess the uniformity of the InS thin film, OM images were taken at several regions. As shown in Figure S5, the as-grown InS bi- or trilayers have good uniformity. According to indirect allowed transition mechanisms,[29, 30] the band gap (E_g) of InS was calculated based on the Tauc relation between incident photon energy ($h\nu$) and the absorption coefficient (α), as below: $\alpha h\nu = B(h\nu - E_g)^2$, in which B is a constant.[31] As shown in Figure 2d, the photon energy function for the bilayer and trilayer InS films is based on the Tauc plot of $(\alpha h\nu)^{1/2}$. The linear approach x-intercepts represent the E_g of ~2.56 eV for the bilayer and ~2.49 eV for the trilayer, respectively, which are in good agreement with previous simulation reports.[6]

The stoichiometry of the CVD InS atomic layers were confirmed by XPS. Figure 2e and f display the In 3d and S 2p spectra at different binding energies, respectively, both of which have clear-fitted doublet binding energies. In particular, two main In 3d peaks (In $3d_{5/2}$ and In $3d_{3/2}$) can be distributed to the binding energies of 444.1 and 451.7 eV, respectively, while the In 3d region has well-separated spin-orbit components (Δ_{metal} = 7.6 eV). It is noteworthy that the XPS In 3d spectrum shows no In_2O_3 peaks at 445.4 eV and 452.8 eV,[32] demonstrating our CVD InS is an oxygen-free crystals. The binding energies of both the S $2p_{3/2}$ and S $2p_{1/2}$ orbitals that correspond to the divalent sulfide ions were identified at 161.3 and 162.5 eV, respectively. Moreover, S−O bonds of 167.6 eV in CVD InS atomic layers were not observed;[33] thus, the possibility of an oxidation reaction in the InS sample was eliminated. This observation is in favorable agreement with the previous report using bulk InS.[13] After further analysis, the stoichiometry of the as-grown InS atomic layers was calculated from the respective within-peak integrated areas. It is worth noting that the element ratio of In:S was 1:1, which means that CVD synthesis exhibits a stable and clearly good InS chemical composition. Moreover, the stoichiometry of the InS atomic layers were double-checked with an energy dispersive X-ray spectroscopy (EDX) in conjunction with TEM. As shown in Figure S6, EDX analysis showed an In:S atomic ratio of ~1. To further reveal the InS phase, a grazing incident X-ray diffraction (GIXRD) was used to characterize the synthesized InS thin film. In Figure S7, the main peak at 2θ = 30.4° is designated as the InS(110) reflection, which matches well with a standard InS

data file (JCPDS 019-0588).[15, 30] At the same time, the obvious (110) plane indicates that the InS film has a higher crystalline quality. After considering the overall AFM, Raman, absorption, XPS, EDX, and XRD properties, the CVD InS atomic layers are found to be quite close to previous bulk or thick-film InS.

For further characterization of the crystal structure and crystalline state of CVD InS, a PMMA-mediated transfer method was used to transfer the as-grown InS flakes from the mica substrate to lacey carbon grid films on copper TEM grids. Figure 3a is an extremely low magnification TEM image that shows the entire profile of trilayer InS flakes where the triangular flake has a layered, continuous, and homogeneous morphology at the microscale. We noticed that some random small folds and cracks may be introduced during the transfer process. Figure 3b displays a selected-area electron diffraction (SAED) pattern of the InS flakes, which exhibits six-fold symmetry while suggesting that CVD InS has the high crystalline quality of a hexagonal lattice. To further examine the quality of these flakes down to the atomic level, an aberration-corrected STEM was used to offer an in-depth analysis of the InS crystallinity. Figure 3c shows a STEM image for the periodic arrangement of CVD InS atoms, showing the perfect crystallinity of synthetic InS flakes with a perfect honeycomb lattice where the In and S atoms can be clearly distinguished. It also shows a hexagonal crystal structure that has a lattice constant a = 3.94 Å along the high-symmetry direction (100); meanwhile, it is consistent with the previous InS-related literature.[21, 22, 34] Furthermore, Figure 3d shows the TEM cross-

sectional morphology of bilayer InS that display distinctive layered structures. The as-grown InS bilayers are sandwiched between an ink passivation layer and a mica substrate where the atom intensity distribution shows that the thickness of the bilayer InS is ~1.7 nm. As could be expected, this is consistent with our AFM results.

In our previous work, the monolayer InSe exposed to ambient conditions oxidized and was degraded within three days.[20] Ultimately, InS's stability needs to be tested in ambient conditions. For environmental control, the temperature range of the room was approximately 25–27°C while relative humidity was 50–60%, and a 18/6 h light/dark cycle was used. Under our experimental conditions, the OM images show distinct contrast levels in InS flakes among different layers and days. Optical contrast showed a linear dependence on the number of days for the bilayer and trilayer InS flakes, for at least three days and 14 days, respectively, as shown in Figure 4. The bilayer CVD InS flakes had completely disappeared within seven days while the trilayer InS maintained their triangular shape for more than 14 days, exhibiting resistance to air and moisture molecules. Under the same ambient conditions, the anti-oxidation performances of the bilayer InS flakes and the monolayer InSe flakes were compared. Each can maintain a triangular profile for about three days, as shown in Figure 4 and S8, but the difference in the number of layers indicates that InS is slightly less stable under oxygen than InSe. This result is consistent with previous simulation reports that the binding energy of InS and oxygen atoms (ΔH= -2.91 eV) is lower than that of InSe and oxygen atoms (ΔH= -2.22 eV).[7]

Finally, the electrical transport properties of CVD InS atomic layers need to be understood precisely to use them in transistor applications. Thus, the setup of an electric double layer transistor (EDLT) in conjunction with single-crystal InS triangular flakes has been analyzed (see Supporting Information, Methods). EDLTs are famous for their accurate mobility determination method at high carrier concentrations, which is a powerful approach and usually used when attaining the oxide dielectric layer is difficult to obtain nice transport properties. The entire EDLT production process for 2D materials has been reported elsewhere.[35-39] Using ion gels as a top gate dielectric layer for InS EDLT, a PS-PMMA-PS triblock copolymer is mixed with an [DEME][TFSI] ionic liquid.[40, 41] The schematic molecular structures of the [DEME][TFSI] and PS-PMMA-PS were depicted as shown in Figure 5a. Moreover, Figure 5b shows an OM image of InS devices where the channel length between the drain and source electrodes is estimated as 25 μm. Both gold electrodes were thermally evaporated upon InS flake tops through a metal hard-mask. The ion gels were directly drop-casted on channel surfaces, and Figure 5c demonstrates the photographs of the InS EDLT device, showing before and after photos for top-gate metal deposition. Figure 5d shows the linear-scale transfer characteristics of a trilayer InS EDLT at room temperature. The n-transfer curve of the trilayer InS EDLT (*i.e.* the electron accumulations induced by positive gate voltage (V_G)) is given while the drain voltage (V_D) is set to 0.1 V for linear regime operations. Meanwhile, we observed that

the average threshold voltage for the forward and reverse scans was ~2 V. When the negative V_G ranging from 0 to -3 V is applied to the devices, only gate leakage current is seriously increased, meaning no hole transport current and demonstrating that InS is an electron-conductive semiconductor. Thus, the unipolar n-type transport of the CVD InS device that was exhibited agrees with the thick InS crystal reported by Nishino et al.[8] In addition, the n-channel I_D is converted from a linear scale to a logarithmic scale, as shown in Figure 5e. Meanwhile, the on-off current ratio of trilayer InS EDLT is over 10^3. The hysteresis in transfer characteristics shown in Figures 5d and 5e might be due to the charge trap effects and/or the adsorption effects on the interface between the ions and InS. Once the electron accumulations (ion redistributions) occur, the chemical potentials and polarity on the interface are also changed accordingly, which could give the slight shifts of threshold voltages for the reverse scan.[42] Another possibility is the scan speed of the V_G. Because the operation frequency of EDLTs strongly depends on ion conductivity, it usually results in slow operation speed of the devices. Although we used a sufficient scan speed (10 mV/s), the slow response of ions may have caused the hysteresis for depletion of accumulated electrons.[35-40] Furthermore, the electron mobility μ is defined by the equation $\mu = (L/WC_iV_D) \cdot (\Delta I_D/\Delta V_G)$ in the linear regime where W is the channel width, L is the channel length, V_G is the gate voltage, V_D is the drain voltage, I_D is the drain current, and C_i is the interface capacitance of InS/ion-gels. Each InS/ion-gel C_i is obtained within the scope of 5–10 μF/cm^2, being very similar to that previously reported in InSe,[20] where

the phase angle is around -85° and the capacitance at the frequency range from 10^1 to 10^2 Hz is approximately constant as shown in Figure 5f. According to the measured interface capacitance, the estimated average electron mobility for the trilayer InS is ~ 0.93 cm^2/Vs (Table I), the fastest being up to ~ 2.0 cm^2/Vs (represented by Figure 5). Figure 5g shows the output characteristics of InS EDLTs for various V_G values, and adequate current amplification is obtained. In particular, the linear regime of V_D ranging from 0 V to 0.1 V exhibits excellent linearity, meaning an acceptable Ohmic-like contact behavior. The intense electric fields due to EDLs can induce steep band bending on the metal/InS interfaces, which significantly reduces contact resistance effects in EDLTs.[35] Despite the Ohmic-like characteristics being observed in Figure 5g, the contact resistance cannot be completely removed; thus, designing ideal contact metal for InS will be an important future subject to further improve device performances.[43] Lastly, electrical performances of EDLTs made with different thicknesses of InS flakes (bilayer and trilayer) are summarized in Table I. We note that for bilayer InS, the electron mobility was reduced to 0.24 cm^2/Vs (see Supporting Information, Figure S9), which is about quadruple lower than the trilayer InS EDLTs. The n-channel threshold voltage shifts from 2.0 V for trilayer InS to 1.75 V for bilayer InS. This also indicates that the bilayer InS results in higher gate control capability and can operate at lower turn-on voltage. In should be noted that the obtained electron mobilities for both bilayer and trilayer InS are still very low. One possible reason for these low mobilities is the effect of surface traps originating from defects and/or

disorders. Indeed, the subthreshold swings, the $S = dV_G/d(\log I_D)$, for bilayer and trilayer InS EDLTs are calculated to be 150 mV/dec and 145 mV/dec, respectively. These values are significantly higher than the ideal S of ~60 mV/dec, indicating that serious trap states existed on the InS surface. Optimizations of growth and transfer conditions, surface treatments, passivation techniques, and substrate engineering will be feasible ways to reduce the trap density and to further enhance mobility. Moreover, introducing In electrodes for contact metal is a promising approach to improve carrier injections for realizing superior mobility.[43-45]

3. Conclusion

In summary, the highly crystalline and large-area InS bilayers and trilayers on mica substrates were synthesized using the precursor-assisted CVD process. The InS samples were characterized using various spectral methods such as Raman, absorption spectroscopy, and XPS. The CVD InS's high crystallinity and hexagonal lattice structure were demonstrated by AFM, TEM, and SAED. Furthermore, the CVD InS device demonstrates native n-type behavior, accompanying the electron mobility of up to ~2 cm^2/Vs and the on-off current ratio over 10^3. In addition, the CVD InS atomic layers were readily transferred to arbitrary substrates, being further extended to next-generation nanoelectronic devices that are more flexible, feature high-transparency, and low-power.

Acknowledgements

This work was supported by the Ministry of Science and Technology, Taiwan, under grant numbers MOST106-2221-E-110-084-MY3 and MOST107-2221-E-110-076-MY3. The authors gratefully acknowledge the use of TEM, XPS, AFM, Raman, FIB, and XRD pieces of equipment belonging to the Instrument Centers of NTHU, NCHU, NCKU, and NSYSU. K.-I L. is grateful for the support of the Ministry of Science and Technology, Taiwan, under grant number MOST107-2112-M-006-017 and MOST108-2112-M-006-010. J.P. was supported by JSPS-KAKENHI grant number JP19K15383. T.T. was supported by JSPS KAKENHI (Grant Numbers JP15K21721, JP26102012, JP25000003, and JP17H01069) and JST CREST (Grant Number JPMJCR17I5).

References

1. K. Xu, L. Yin, Y. Huang, T. A. Shifa, J. Chu, F. Wang, R. Cheng, Z. Wang and J. He, *Nanoscale*, 2016, **8**, 16802-16818.
2. W. Huang, L. Gan, H. Li, Y. Ma and T. Zhai, *CrystEngComm*, 2016, **18**, 3968-3984.
3. Z. Yang and J. Hao, *Advanced Materials Technologies*, 2019, **4**, 1900108.
4. H. Cai, Y. Gu, Y.-C. Lin, Y. Yu, D. B. Geohegan and K. Xiao, *Applied Physics Reviews*, 2019, **6**, 041312.
5. K. Yuan, R. Yin, X. Li, Y. Han, M. Wu, S. Chen, S. Liu, X. Xu, K. Watanabe, T. Taniguchi, D. A. Muller, J. Shi, P. Gao, X. Wu, Y. Ye and L. Dai, *Advanced Functional Materials*, 2019, **0**, 1904032.
6. D. Wickramaratne, F. Zahid and R. K. Lake, *J. Appl. Phys.*, 2015, **118**, 075101.
7. S. Zhou, C.-C. Liu, J. Zhao and Y. Yao, *npj Quantum Mater.*, 2018, **3**, 16.
8. T. Nishino and Y. Hamakawa, *Japanese Journal of Applied Physics*, 1977, **16**, 1291-1300.
9. D. A. Bandurin, A. V. Tyurnina, G. L. Yu, A. Mishchenko, V. Zólyomi, S. V. Morozov, R. K. Kumar, R. V. Gorbachev, Z. R. Kudrynskyi, S. Pezzini, Z. D. Kovalyuk, U. Zeitler, K. S. Novoselov, A. Patanè, L. Eaves, I. V. Grigorieva, V. I. Fal'ko, A. K. Geim and Y. Cao, *Nat. Nanotechnol.*, 2016, **12**, 223-227.
10. P.-H. Ho, Y.-R. Chang, Y.-C. Chu, M.-K. Li, C.-A. Tsai, W.-H. Wang, C.-H. Ho, C.-W. Chen and P.-W. Chiu, *ACS Nano*, 2017, **11**, 7362-7370.
11. N. Balakrishnan, E. D. Steer, E. F. Smith, Z. R. Kudrynskyi, Z. D. Kovalyuk, L. Eaves, A. Patanè and P. H. Beton, *2D Mater.*, 2018, **5**, 035026.
12. C.-H. Ho, Y.-H. Chen and J.-H. Ho, *RSC Advances*, 2016, **6**, 97445-97448.
13. Y. Wang, K. Szökölová, M. Z. M. Nasir, Z. Sofer and M. Pumera, *ChemCatChem*, 2019,

11, 2634-2642.

14. J. A. Hollingsworth, D. M. Poojary, A. Clearfield and W. E. Buhro, *Journal of the American Chemical Society*, 2000, **122**, 3562-3563.
15. T. Wang, J. Wang, J. Wu, P. Ma, R. Su, Y. Ma and P. Zhou, *Nanomaterials*, 2019, **9**, 865.
16. A. Y. Zavrazhnov, A. V. Naumov, P. V. Anorov, E. G. Goncharov, V. I. Sidei and V. S. Pervov, *Inorganic Materials*, 2006, **42**, 1294-1298.
17. A. Y. Zavrazhnov, A. V. Kosyakov, A. V. Naumov, A. V. Sergeeva and S. S. Berezin, *Thermochimica Acta*, 2013, **566**, 169-174.
18. Ming-Yang Li, Sheng-Kai Su, H-S Philip Wong and L.-J. Li, *Nature*, 2019, **567**, 169-170.
19. H. Li, J.-K. Huang, Y. Shi and L.-J. Li, *Advanced Materials Interfaces*, 2019, **0**, 1900220.
20. H.-C. Chang, C.-L. Tu, K.-I. Lin, J. Pu, T. Takenobu, C.-N. Hsiao and C.-H. Chen, *Small*, 2018, **14**, 1802351.
21. S. Demirci, N. Avazlı, E. Durgun and S. Cahangirov, *Phys. Rev. B*, 2017, **95**, 115409.
22. V. Zólyomi, N. D. Drummond and V. I. Fal'ko, *Phys. Rev. B*, 2014, **89**, 205416.
23. N. M. Gasanly, H. Özkan, A. Aydinli and İ. Yilmaz, *Solid State Commun.*, 1999, **110**, 231-236.
24. R. Kumaresan, M. Ichimura, N. Sato and P. Ramasamy, *Materials Science and Engineering: B*, 2002, **96**, 37-42.
25. W. Huang, L. Gan, H. Yang, N. Zhou, R. Wang, W. Wu, H. Li, Y. Ma, H. Zeng and T. Zhai, *Advanced Functional Materials*, 2017, **27**, 1702448.
26. C. Cui, W.-J. Hu, X. Yan, C. Addiego, W. Gao, Y. Wang, Z. Wang, L. Li, Y. Cheng, P. Li, X. Zhang, H. N. Alshareef, T. Wu, W. Zhu, X. Pan and L.-J. Li, *Nano Lett.*, 2018, **18**, 1253-1258.
27. Q. Ji, Y. Zhang, T. Gao, Y. Zhang, D. Ma, M. Liu, Y. Chen, X. Qiao, P.-H. Tan, M. Kan, J. Feng, Q. Sun and Z. Liu, *Nano Lett.*, 2013, **13**, 3870-3877.
28. Y.-H. Chang, W. Zhang, Y. Zhu, Y. Han, J. Pu, J.-K. Chang, W.-T. Hsu, J.-K. Huang, C.-L. Hsu, M.-H. Chiu, T. Takenobu, H. Li, C.-I. Wu, W.-H. Chang, A. T. S. Wee and L.-J. Li, *ACS Nano*, 2014, **8**, 8582-8590.
29. J. Jalilian and M. Safari, *Physics Letters A*, 2017, **381**, 1313-1320.
30. E. GÜNERİ and F. GÖDE, *Turkish Journal of Physics*, 2017, **41**, 359-366.
31. A. S. Hassanien and A. A. Akl, *Superlattices Microstruct.*, 2016, **89**, 153-169.
32. B. Nilanthy, R. K. Zakhar, F. S. Emily, W. F. Michael, M. Oleg, D. K. Zakhar, E. Laurence, H. B. Peter and P. Amalia, *2D Mater.*, 2017, **4**, 025043.
33. W. Yuan, L. Cheng, Y. An, S. Lv, H. Wu, X. Fan, Y. Zhang, X. Guo and J. Tang, *Advanced Science*, 2018, **5**, 1700870.

34. H. L. Zhuang and R. G. Hennig, *Chem. Mater.*, 2013, **25**, 3232-3238.
35. J.-K. Huang, J. Pu, C.-L. Hsu, M.-H. Chiu, Z.-Y. Juang, Y.-H. Chang, W.-H. Chang, Y. Iwasa, T. Takenobu and L.-J. Li, *ACS Nano*, 2014, **8**, 923-930.
36. J. Pu, L.-J. Li and T. Takenobu, *Phys. Chem. Chem. Phys.*, 2014, **16**, 14996-15006.
37. C.-H. Chen, C.-L. Wu, J. Pu, M.-H. Chiu, P. Kumar, T. Takenobu and L.-J. Li, *2D Mater.*, 2014, **1**, 034001.
38. J. Pu, T. Fujimoto, Y. Ohasi, S. Kimura, C.-H. Chen, L.-J. Li, T. Sakanoue and T. Takenobu, *Adv. Mater.*, 2017, **29**, 1606918.
39. J. Pu, K. Kanahashi, N. T. Cuong, C.-H. Chen, L.-J. Li, S. Okada, H. Ohta and T. Takenobu, *Phys. Rev. B*, 2016, **94**, 014312.
40. J. Pu, Y. Yomogida, K.-K. Liu, L.-J. Li, Y. Iwasa and T. Takenobu, *Nano Lett.*, 2012, **12**, 4013-4017.
41. Y. Kawasugi, K. Seki, Y. Edagawa, Y. Sato, J. Pu, T. Takenobu, S. Yunoki, H. M. Yamamoto and R. Kato, *Nat. Commun.*, 2016, **7**, 12356.
42. H. Yuan, H. Shimotani, A. Tsukazaki, A. Ohtomo, M. Kawasaki and Y. Iwasa, *Journal of the American Chemical Society*, 2010, **132**, 6672-6678.
43. B. Shi, Y. Wang, J. Li, X. Zhang, J. Yan, S. Liu, J. Yang, Y. Pan, H. Zhang, J. Yang, F. Pan and J. Lu, *Phys. Chem. Chem. Phys.*, 2018, **20**, 24641-24651.
44. M. Li, C.-Y. Lin, S.-H. Yang, Y.-M. Chang, J.-K. Chang, F.-S. Yang, C. Zhong, W.-B. Jian, C.-H. Lien, C.-H. Ho, H.-J. Liu, R. Huang, W. Li, Y.-F. Lin and J. Chu, *Adv. Mater.*, 2018, **30**, 1803690.
45. Y.-T. Huang, Y.-H. Chen, Y.-J. Ho, S.-W. Huang, Y.-R. Chang, K. Watanabe, T. Taniguchi, H.-C. Chiu, C.-T. Liang, R. Sankar, F.-C. Chou, C.-W. Chen and W.-H. Wang, *ACS Appl. Mater. Interfaces*, 2018, **10**, 33450-33456.

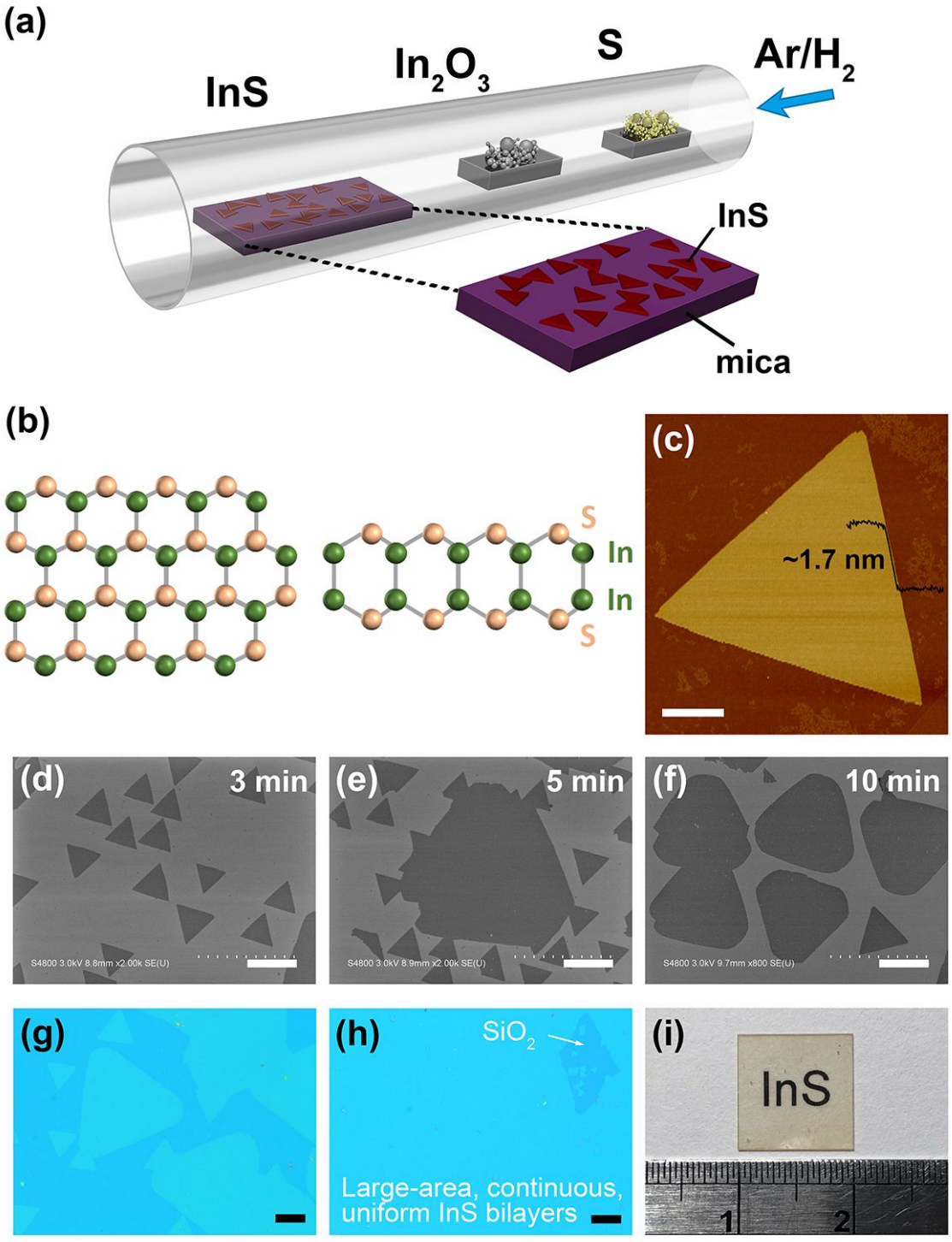

Figure 1. (a) Schematic diagram of experimental setup for CVD synthesis of InS atomic layers. (b) Top and side schematics of the InS crystal structure. Green and gold spheres correspond to indium and sulfur atoms, respectively. (c) AFM image of bilayer InS flake. Scale bar, 10 μm. (d-f) Low-magnification SEM images of the bilayer InS flakes at growth times of 3, 5, and 10 min. Scale bar, 10, 10, 25 μm respectively. (g, h) OM images of the InS bilayer flakes and films. Scale bar, 10 μm. (i) Photograph of centimeter-scale bilayer InS film synthesized on a transparent mica substrate, showing highly uniform.

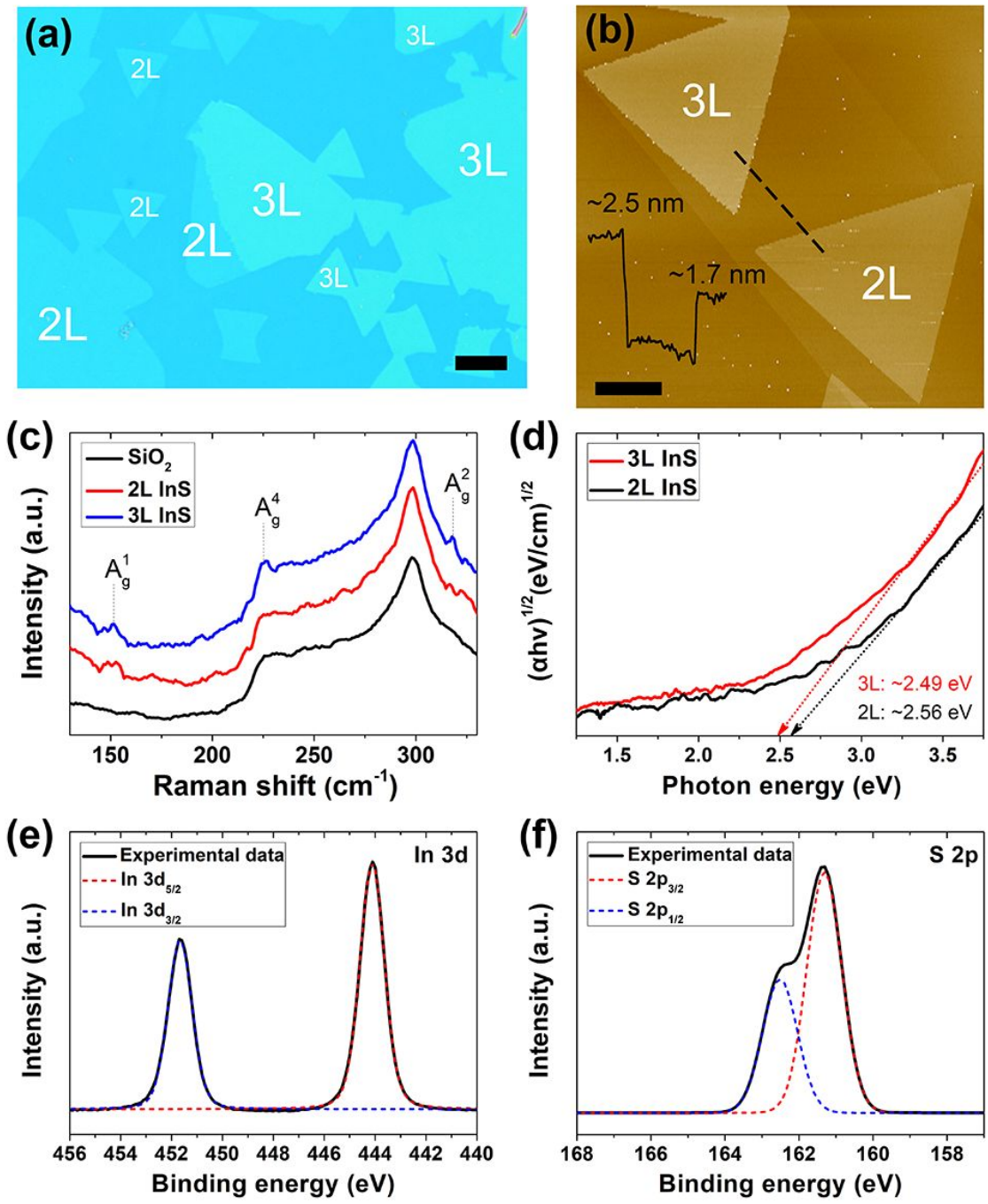

Figure 2. (a) OM and (b) AFM images of trilayer InS grown on certain of those bilayer top. Scale bar, 10 μm. (c) Raman spectra of bi- and trilayer InS flakes, excited by a 488 nm laser. (d) Plots of the $(\alpha h\nu)^{1/2}$ versus photon energy ($h\nu$) for indirect interband transitions of the continuous bi- and trilayer InS films whose x-intercepts represent the band gap energy. (e, f) XPS spectra of InS film, in which the (e) In 3d core level and (f) S 2p core level binding energies are identified.

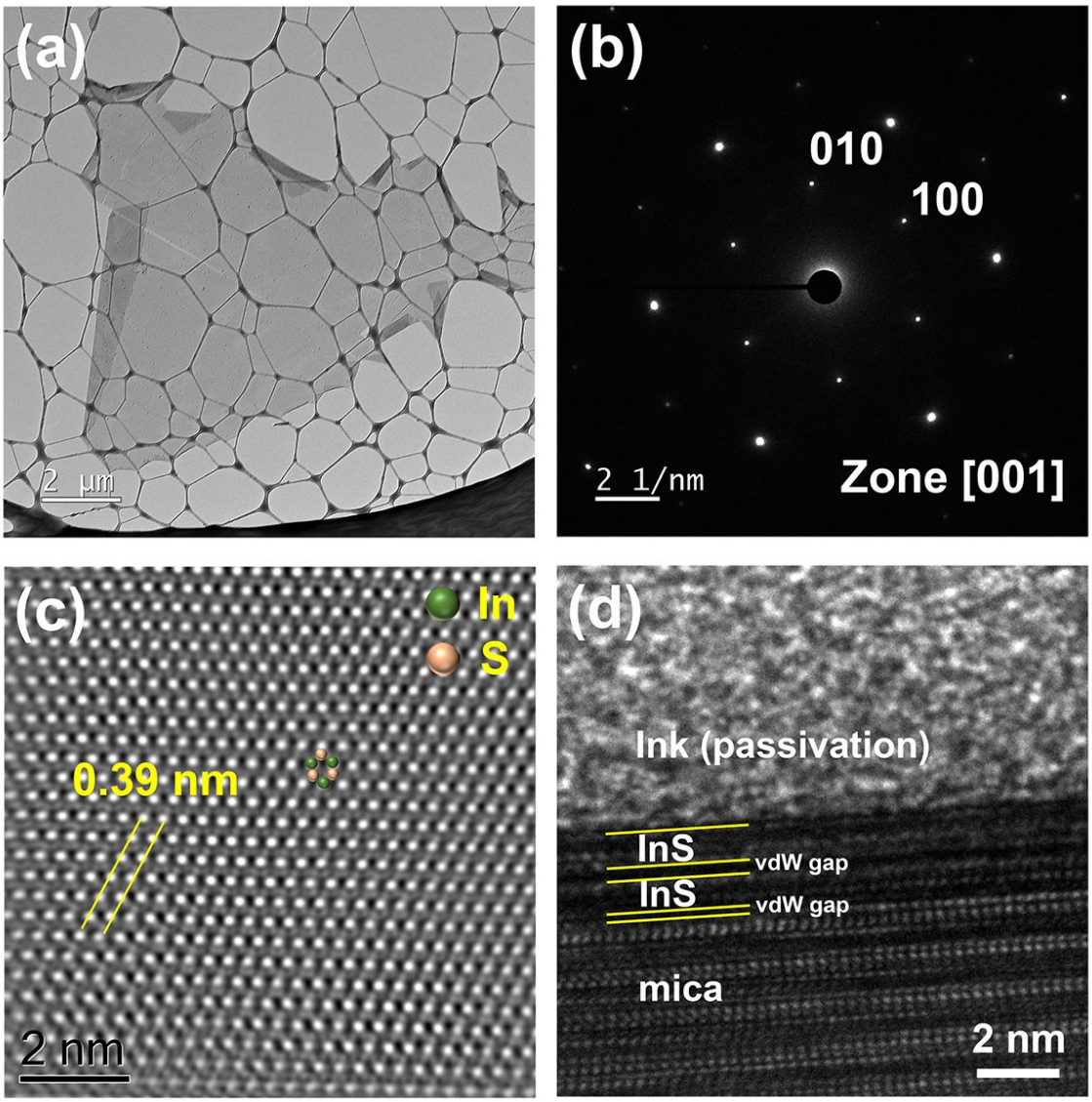

Figure 3. (a) Low-resolution TEM image of the trilayer InS flakes with triangular nanostructure and (b) its SAED pattern. (c) High-resolution HAADF STEM image of trilayer InS, where the In and S atoms are identified. (d) Cross-section TEM image of a bilayer InS film.

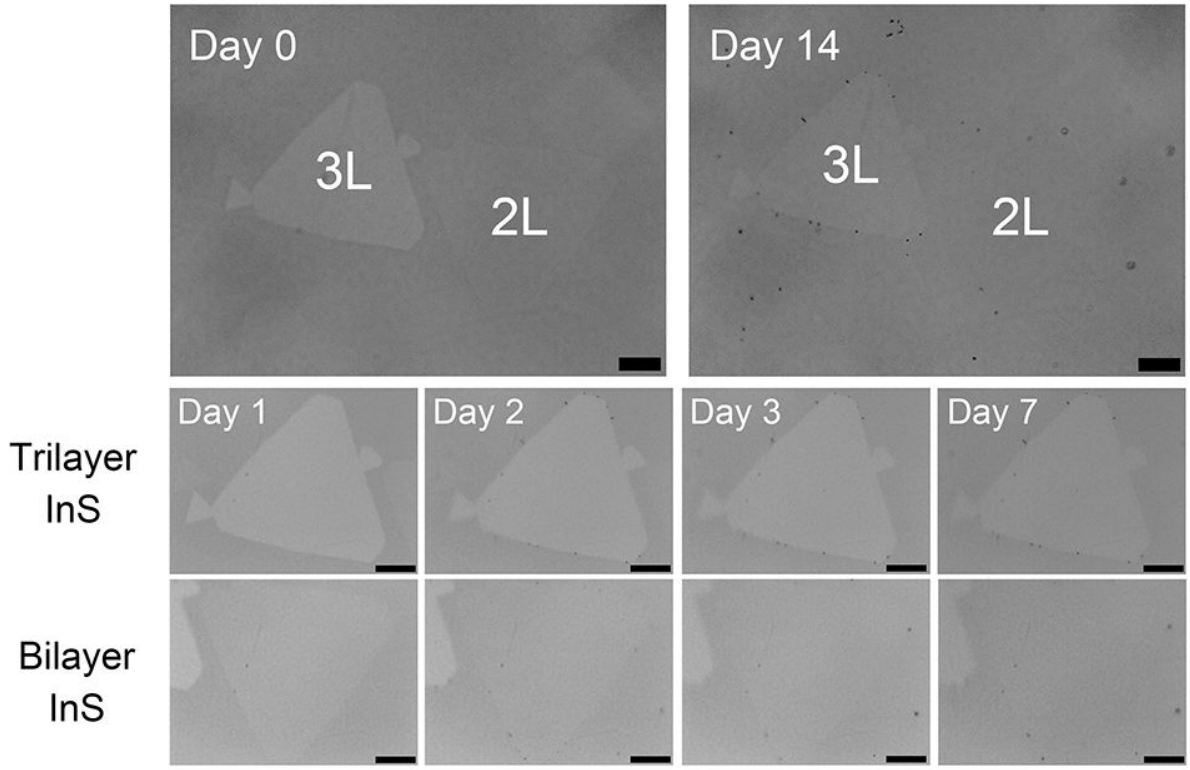

Figure 4. Sequence of OM images acquired at different times for comparison of the stability of bi- and trilayer InS under ambient conditions. (Day n: after exposure to ambient conditions n days). Scale bar is 10 μm in length.

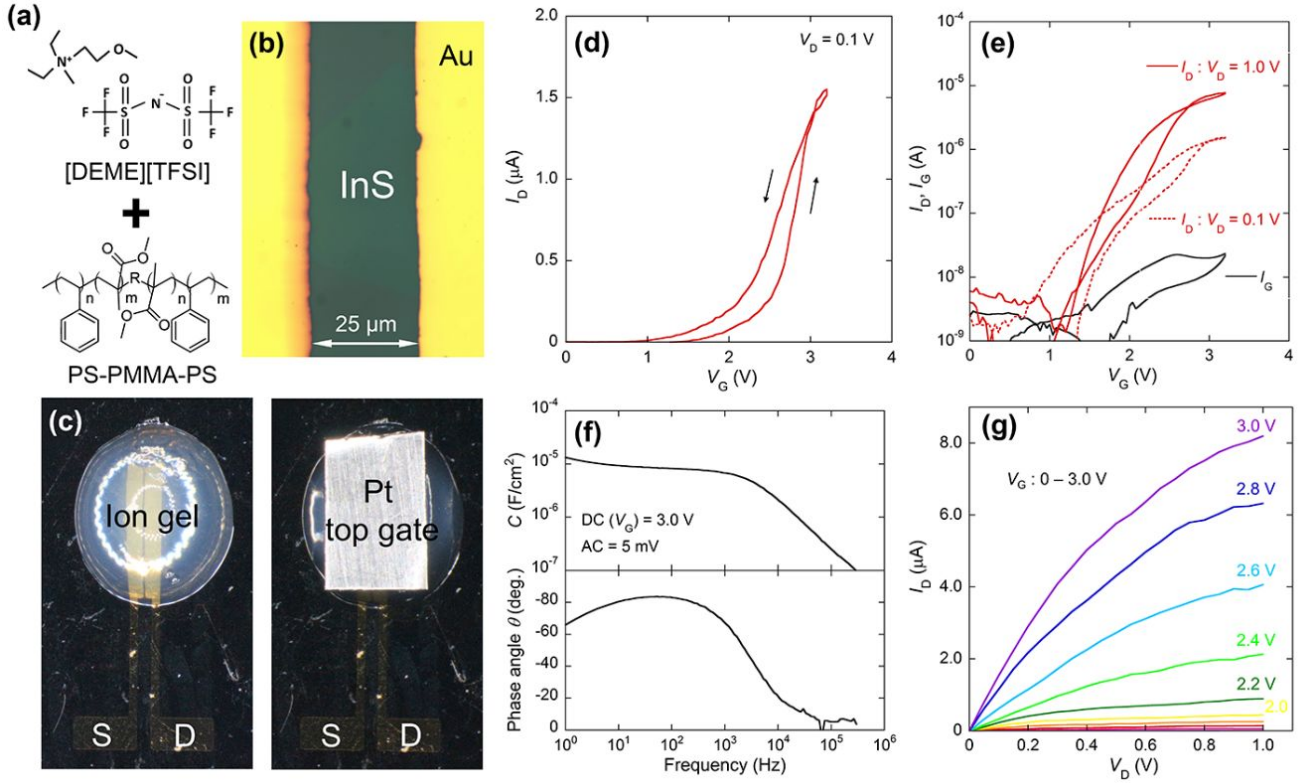

Figure 5. (a) Schematic molecular structures of the [DEME][TFSI] and PS-PMMA-PS for ion gel. (b) Top view OM image of the InS EDLT constructed on a SiO_2/Si substrate, where the Au source/drain electrodes were stacked on trilayer InS flakes. (c) Top view OM image of the InS EDLT device, which were taken before and after the ion gel and top gate stacking. (d) Linear scale and (e) Logarithmic-scale transfer curves of the InS EDLT. The V_D of 0.1 V and 1.0 V were shown by red, and the I_G for V_D of 0.1 V was also displayed by gray. (f) The frequency dependence of the specific capacitance and the phase angle for InS EDLT. (g) Output characteristics of the InS EDLT with Au top-contact electrode. The V_G was varied from 0 V to 3.0 V.

TABLE I. Summarization of the InS Samples from EDLT Measurements

InS samples	Polarity	V_{th} (V)	On-off ratio	μ (cm^2/Vs)
Bilayer	n-type	1.75	10^3	0.24
Trilayer	n-type	2	10^3–10^4	0.93*

* The highest mobility reached 2 cm^2/Vs

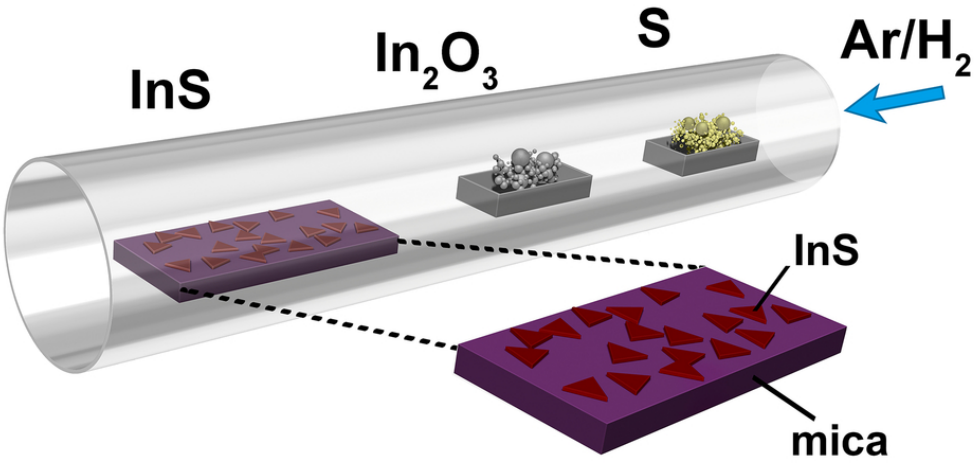

A table of contents entry

80x40mm (300 x 300 DPI)